DOI: 10.1002/ange.201400457

Flexible Conducting Materials

Macroscopic Free-Standing Hierarchical 3D Architectures Assembled from Silver Nanowires by Ice Templating**

*Huai-Ling Gao, Liang Xu, Fei Long, Zhao Pan, Yu-Xiang Du, Yang Lu, Jin Ge, and Shu-Hong Yu**

Abstract: *As macroscopic three dimensional (3D) architectures show increasing significance, much effort has been devoted to the hierarchical organization of 1D nanomaterials into serviceable macroscopic 3D assemblies. How to assemble 1D nanoscale building blocks into 3D hierarchical architectures is still a challenge. Herein we report a general strategy based on the use of ice as a template for assembling 1D nanostructures with high efficiency and good controllability. Free-standing macroscopic 3D Ag nanowire (AgNW) assemblies with hierarchical binary-network architectures are then fabricated from a 1D AgNW suspension for the first time. The microstructure of this 3D AgNW network endows it with electrical conductivity and allows it to be made into stretchable and foldable conductors with high electromechanical stability. These properties should make this kind of macroscopic 3D AgNW architecture and it composites suitable for electronic applications.*

One-dimensional (1D) nanostructures have shown great application potential in electronics, optoelectronics, bioelectronics, and molecular sensing devices[1] owing to their anisotropic nature associated with their functionalities. The problem of how to effectively assemble nanoscale building blocks including 1D nanostructures into macroscopic functional architectures has become increasingly important from the viewpoint of practical applications.[2] Much effort has been devoted to the hierarchical organization of 1D nanostructures into serviceable macroscopic assemblies for desired applications, among which, assemblies with three-dimensional (3D) architectures are demonstrating increasingly significance.[3] For example, Lieber et al.[3a] have prepared macroporous, flexible, and free-standing nanowire nanoelectronic scaffolds. The 3D architectures obtained can monitor in real-time the physicochemical and biological microenvironments throughout their 3D and macroporous interior, such materials can have a marked impact in both electronics and biomaterials. Suh et al.[3b] have fabricated a flexible strain-gauge sensor using two interlocked arrays of conductive nanofibers. This kind of hierarchical assembly can detect pressure, shear, and torsion with high sensitivity. Wang et al.[3i] use ZnO nanowire arrays to convert mechanical energy into electricity and a solely nanowire-based, self-powered nanosensor unit was demonstrated. These remarkable achievements inspired us to build nanoscale building blocks into higher hierarchically assembled architectures with fascinating structures and potential applications. The present large-scale assembly techniques for assembling these nanostructures into highly ordered, aligned, and regular two-dimensional film structures have been readily realized.[2a–f,4] Yet, with respect to the fabrication of 3D nanowire architectures, the synthesis strategies are mainly based on direct growth of complex nanowire arrangements[3g–k,5] or the assembly of unordered nanowire aerogels.[3c–f] The preparation processes of 3D ordered nanowire architectures by the direct growth method are commonly time-consuming and need harsh synthesis conditions. With respect to the unordered 3D nanowire aerogels, they should demonstrate inferior application properties compared to those 3D nanowire architectures with more organized structures. A challenge, therefore, still facing practical application is the large-scale and efficient assembly of 1D nanowires into more complicated and hierarchical 3D architectures with controlled organization, orientation, spacing, and ultimately providing a useful system.

Herein, we report a general, versatile assembly technique which has high efficiency and controllability, using an ice-template approach to convert directly assembled monodispersed silver nanowires (AgNWs) into free-standing macroscopic 3D cellular-like architectures without using any extra functionalization agent or crosslinking agent for the first time. The 3D monoliths obtained have a hierarchical binary-network architecture (2D nano-networks of AgNWs compartmental films and 3D AgNW micro-networks of the interconnected compartmental units).[6] The unique binary-network microstructure endows this kind of 3D nanowire architecture with structural stability under a certain extent of

[*] Dr. H. L. Gao,[+] Dr. L. Xu,[+] Z. Pan, Y. X. Du, Dr. Y. Lu, Dr. J. Ge, Prof. Dr. S. H. Yu
Division of Nanomaterials & Chemistry, Hefei National Laboratory for Physical Sciences at Microscale, Collaborative Innovation Center of Suzhou Nano Science and Technology, Department of Chemistry
CAS Key Laboratory of Mechanical Behavior and Design of Materials, University of Science and Technology of China
Hefei, Anhui 230026 (P. R. China)
E-mail: shyu@ustc.edu.cn
Homepage: http://staff.ustc.edu.cn/~yulab/
F. Long
Hefei National Laboratory for Physical Sciences at the Microscale
School of Life Sciences
University of Science and Technology of China
Hefei 230027 (P. R. China)
[+] These authors contributed equally to this work.

[**] This work is supported by the Ministry of Science and Technology of China, the National Basic Research Program of China (Grants 2012BAD32B05-4, 2010CB934700, 2013CB933900, 2014CB931800), the National Natural Science Foundation of China (Grants 91022032, 91227103, 21061160492, J1030412), and the Chinese Academy of Sciences (Grant KJZD-EW-M01-1).
Supporting information for this article is available on the WWW under http://dx.doi.org/10.1002/anie.201400457.

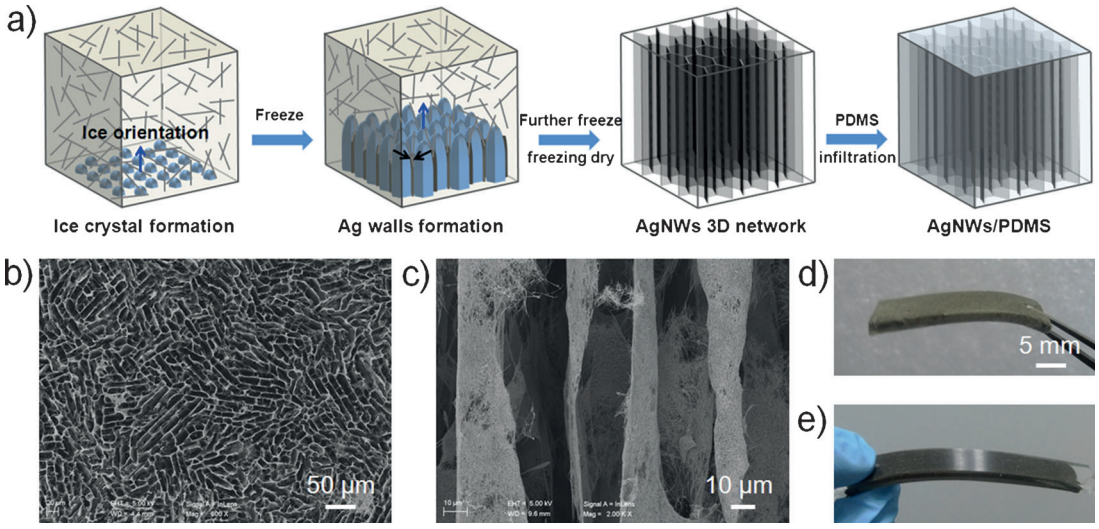

Figure 1. Formation mechanism and morphology of the 3D AgNW compartmentalized architecture. a) Schematic showing the formation mechanism of the compartmental monolith by freeze casting. b,c) Typical top-view (b) and side-view (c) SEM images of AgNWs networks. d,e) Photos of the 3D AgNW monolith and AgNWs/PDMS composite.

deformation.[6] Remarkably, the 3D monoliths obtained can reach a very high electrical conductivity of 50 S cm^{-1} with an ultralow AgNW density. As one potential application, we made this unique binary-network architecture into stretchable and foldable conductor[6,7] and its electromechanical stability was demonstrated.

Fabrication of such a macroscopic 3D AgNW compartmentalized architecture is illustrated in Figure 1. Unidirectional freezing as a straightforward, low-cost, scalable assembly technique was applied[8] as the building process to construct monodispersed AgNW into highly ordered complex structures. High-quality AgNWs with lengths of 4–15 μm (Supporting Information, Figure S1) were used as building blocks. The formation of such a highly ordered compartmental architecture is generated by the oriented growth of ice crystals in the suspension of AgNWs.[9] In brief, when the AgNW suspension is poured into a mold on the precooled plate, fast nucleation of ice crystals will occur randomly on the freezing surface at temperatures far below the freezing point of the solution. Afterwards, ice crystals sweep along with the solidification front to form parallel ice fingers and at the same time the separated AgNWs are pushed together into the interfinger spaces by the growing ice fingers. In this way, interconnect 2D networks of AgNW films were formed among the ice fingers and all the 2D AgNW network films connect together to form an interconnected 3D AgNW compartmental micro-networks. After the ice is sublimed by freeze drying, a macroscopic free-standing monolith of a continuous and interconnected binary-network with well-ordered compartmental architecture can be obtained (Figure 1 d, Figure 2, Figure 3; Supporting Information, Figure S2).

To construct free-standing macroscopic 3D AgNW architectures, a sufficient amount of AgNW building blocks is indispensable. Suspensions with different concentrations of AgNWs were investigated at the same freezing temperature to observe the effect on the microstructures. Free-standing 3D AgNW networks with different density can be obtained without any collapse during the drying process when the initial concentration of the AgNW suspension is no less than 10 mg mL^{-1}. That is to say, it is difficult to form sufficient contacts between AgNWs to support the ultimate 3D network when there were insufficient AgNW building blocks. The scanning electron microscope (SEM) images of the fracture surface of the networks show that the 3D AgNW network is discontinuous when a low concentration of AgNWs was applied, and the 2D AgNW network films become more complete and dense with increasing the amount of AgNWs in the suspensions (Figure 2, Supporting Information Figure S2a–c and Figure S3).

This ice-template assembly method demonstrates great flexibility in controlling both the macrostructure and the microstructure of 3D AgNW architectures. The macrostructure can be simply altered by using molds with different shapes. As the temperature of the freezing surface is the key point to determine the size of the initial ice crystals, which in turn control in the ultimate pore size of the scaffolds,[9] the microstructure and pore structures of 3D AgNW network can be tuned by using different freezing temperature. The SEM images of the fracture surface of the networks show that the reducing of the freezing temperature leads to a decrease in the pore size but an increase in the pore numbers (Figure 3, Supporting Information Figure S2d–f). Furthermore, as indicated in Figure 3 and Figure S2d–f, the 2D AgNW network films become thinner as the freezing temperature reduced from −10 °C to −50 °C. When lower freezing temperature was used, ice crystals grow faster and more and smaller initial ice crystals would form, which then lead to thinner ice crystals in the AgNW suspensions.[9] In this process, AgNWs in the suspensions migrate to the boundaries of more ice crystals, and more compartment are formed. So the 2D AgNW compartmental films should become thinner when the compartment numbers increased but the amount of AgNWs is not increased accordingly. Temperatures above −10 °C and below −50 °C were also studied and compartment width

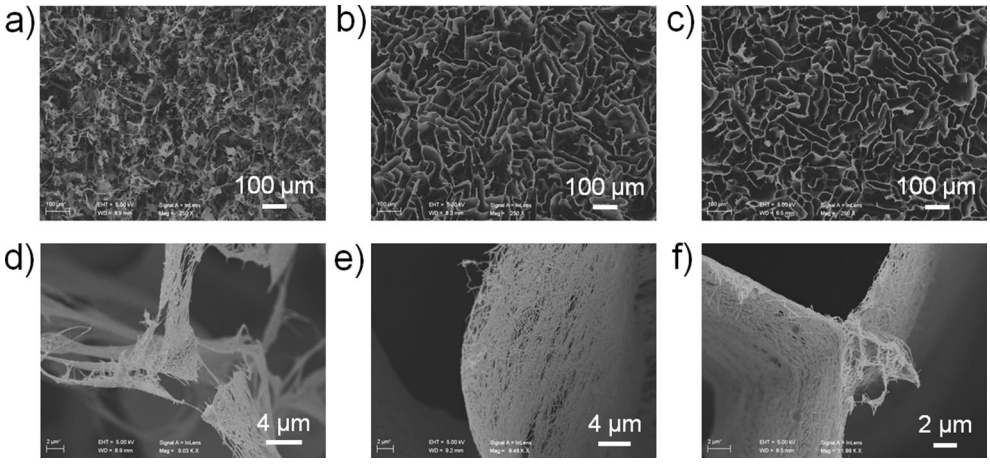

Figure 2. Microstructure of the 3D AgNW compartmental architectures with different amount of AgNWs prepared at −10 °C. a–c) Top-view SEM images of monoliths with a density of a) 10, b) 25, and c) 40 mg cm^{-3}. d–f) Higher magnification images of (a–c).

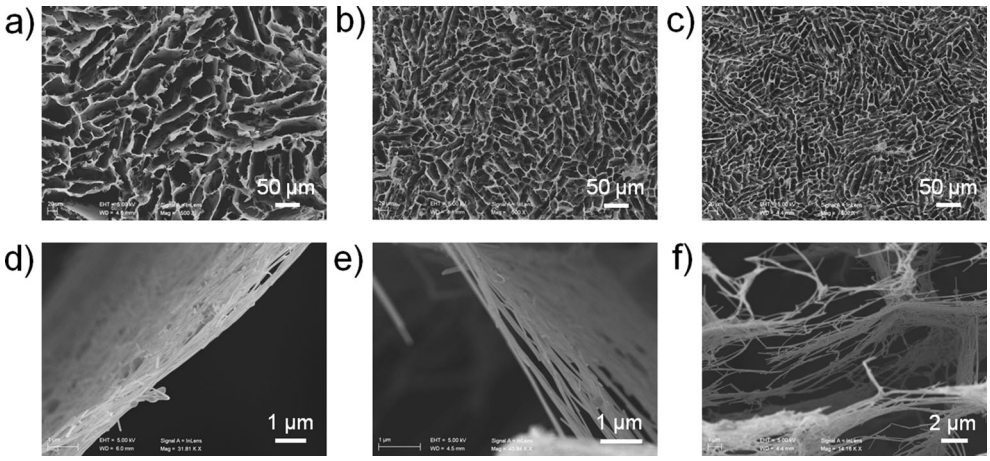

Figure 3. Microstructure of the 3D AgNW compartmentalized architectures prepared by different freezing temperature. a–c) Top-view SEM images of monoliths with a density of 25 mg cm^{-3} prepared at a) −10, b) −30, c) −50 °C. d–f) Higher magnification images of (a–c).

distribution of the assemblies obtain from −5 °C to −196 °C (liquid nitrogen) are displayed in Figure S4. More interestingly, this strategy can also be extend to assemble other one-dimensional nanomaterials into macroscopic free-standing 3D compartmentalized architectures, such as copper nanowires (Supporting Information, Figure S5).

As silver nanowires are one of the best electric materials,[1b] this unique interconnected network of AgNWs should have excellent electrical performance. The electric resistances of the 3D AgNW networks prepared with different conditions (the amount of AgNWs and freezing temperature) were measured. As revealed in Figure S6, the resistance decreased rapidly when the density of AgNWs was increased owing to the presence of more inter-wire junctions, and also showed a linear dependence with the freezing temperature used in the preparation. The results show that the electrical conductivity has a close relationship with the microstructures of 3D AgNW networks.

For networks made with the same amount of AgNWs but a lower preparation temperature, the 2D AgNW network films become increasingly thinner and the number of compartments in the whole monolith increase. Thus the number of paths electrons could take increased in the 3D networks with more compartmental units. As a result the electrical conductivity increases with the reducing freezing temperature. This fact can be used to influence the final electrical conductivity of the 3D networks. The networks can reach a very high electrical conductivity 21.5 S cm^{-1} at an ultra-low density of 25 mg cm^{-3}. This conductivity value is much higher than that of the 3D aerogel-based conductive materials (Supporting Information, Table S1), demonstrating great advantages of our hierarchical 3D AgNW binary-network architecture in electrical applications. The superior electrical conductivity should be attributed to the unblocked electron migration through the infinite interconnected network of high-conductive AgNWs.

To further display the structural advantage of the binary-network architecture in electrical applications, we infiltrate AgNW networks with polydimethylsiloxane (PDMS) to fabricate AgNWs/PDMS composites (Figure 1 e). Importantly, the macrostructure of the 3D AgNW network was not affected at the infiltrating and curing process, as demonstrated by optical microscope and SEM images of the cross section of AgNWs/PDMS composites film (Figure 4 a–d). Compared the electrical conductivity of the initial AgNW networks to that of AgNWs/PDMS composites, nearly no change was observed (about 12.5 S cm^{-1} at the AgNW density of 25 mg cm^{-3} prepared at −10 °C), indicating that introduction of the PDMS matrix does not damage the microstructure of the interconnected 3D network. The microstructure variation of AgNWs/PDMS composites under tensile strength was studied by optical microscopy. As shown in Figure 4 a–c, when the tensile strain on AgNWs/PDMS composite increased from 0–80 %, the macropores of compartmental units (marked by the red window) shrank perpendicular to the direction of the tensile force and elongated in the direction of the applied force. At the microscale, the deformation and elongation of the 3D compartmental units guarantees a continuance of the

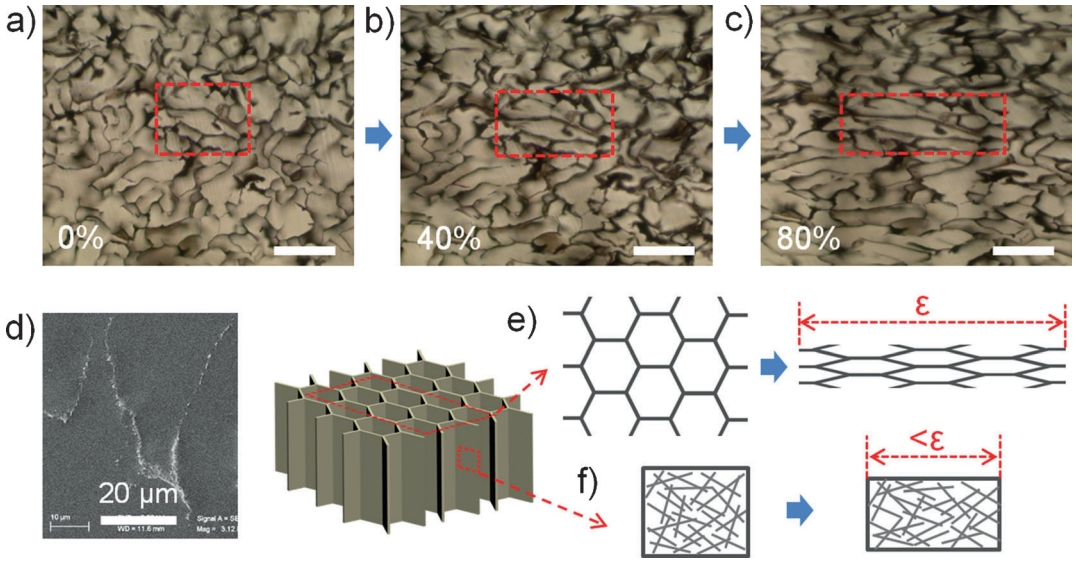

Figure 4. a–c) Optical microscope images of 3D AgNWs/PDMS composite at 0%, 40%, and 80% strain, respectively. All the scale bars are 100 μm. Red windows highlight the changing size of the macropores) Cross section SEM image of 3D AgNW network embedded in a PDMS matrix. The white part indicates the cross section of the 2D AgNW films. e,f) Illustration of effects of elongation on the AgNWs/PDMS micro-network (e) and the 2D AgNW nano-network (f) of the composite under tensile strain (ε).

conductive network in the PDMS, which would protect contacts among AgNWs in the 2D compartmental films from quick disconnection. At the nanoscale, a fine interconnected AgNW network in the 2D compartmental films embedded in PDMS can also effectively accommodate the deformation without a significant decay in conductivity under stretching. The unique binary-network microstructure should offer the great advantage of structural stability under a certain extent of deformation.

The deformation mechanism of the binary network during stretching is shown in Figure 4e,f. Although the composite was elongated to a certain strain (ε) under the tensile strength, the tensile strain observed in AgNW networks in the 2D compartmental films is smaller than ε due to the shape deformation of the 3D compartments. In other words, the tensile strain applied to the AgNW nano-networks of the 3D binary-network architecture was shared by the 3D compartments. Therefore, the 3D nanowire binary-network architectures we prepared should have a better performance in electrical applications than the 2D nanowire networks.

The structural advantages of the 3D binary-network architecture and extraordinary electrical conductivity combines with the excellent mechanical robustness of PDMS make the AgNWs/PDMS composite an appropriate candidate for use as flexible and stretchable conductors (Figure 5).[10] 3D AgNW networks with a density of 25 mg cm^{-3} were chosen to make stretchable conductors and the electrical resistance with respect to stretching strain and bending radius were investigated, which were carried out with a high-precision mechanical system (Instron 5565A).

We first investigated the stretchability of the composites, and the resistance revealed a steep increase in the continuous stretching process (Figure 5a). Note that the composite remained conductive with the resistance change of only about 2 Ω until it broke at 140% strain (Figure 5a). In addition, during the first stretching, the resistance increase ($\Delta R/R_0$) of our AgNWs/PDMS composites at the strain of 100% was about 150%, which is better than other reported flexible conductors based on AgNWs (Supporting Information, Table S2).[6] The resistance variation as a function of uniaxial tensile strain from 0 to 50% was then investigated. As revealed in Figure 5b, the resistance of the AgNWs/PDMS composite increases with increasing tensile strain during the first cycle of stretching, while becomes nearly stable from the second cycle of stretch-release. The irreversible resistance increase is only about 0.3 Ω under 50% stretching (Inset in Figure 5b) and becomes larger for a larger tensile strain (Supporting Information, Figure S7). Even after one-thousand stretch–release cycles the AgNWs/PDMS composites did not show any obvious irreversible resistance increase (Supporting Information, Figure S8). These results can be reasonably attributed to the partial irreversible separation between the AgNWs in the network.

We further investigated the resistance variation under bending deformations. As displayed in Figure 5c,d, the resistance showed a slight increase of less than 0.1 Ω at a bending radius of 2.0 mm during the first bending cycle, and can almost recover after straightening (Figure 5c). Notably, even after 5000 cycles for a bend radius of 2.0 mm, the resistance variation of composites is just less than 0.2 Ω (Figure 5d and inset). These results are a good demonstration of the excellent electromechanical stability of AgNWs/PDMS composites and their great potential for high-performance stretchable and flexible conductors.

In conclusion, we have successfully assembled 1D silver nanowires into free-standing complex macroscopic hierarchical 3D architectures by ice-templating assembly method. The 3D AgNW networks prepared by this approach have a fasci-

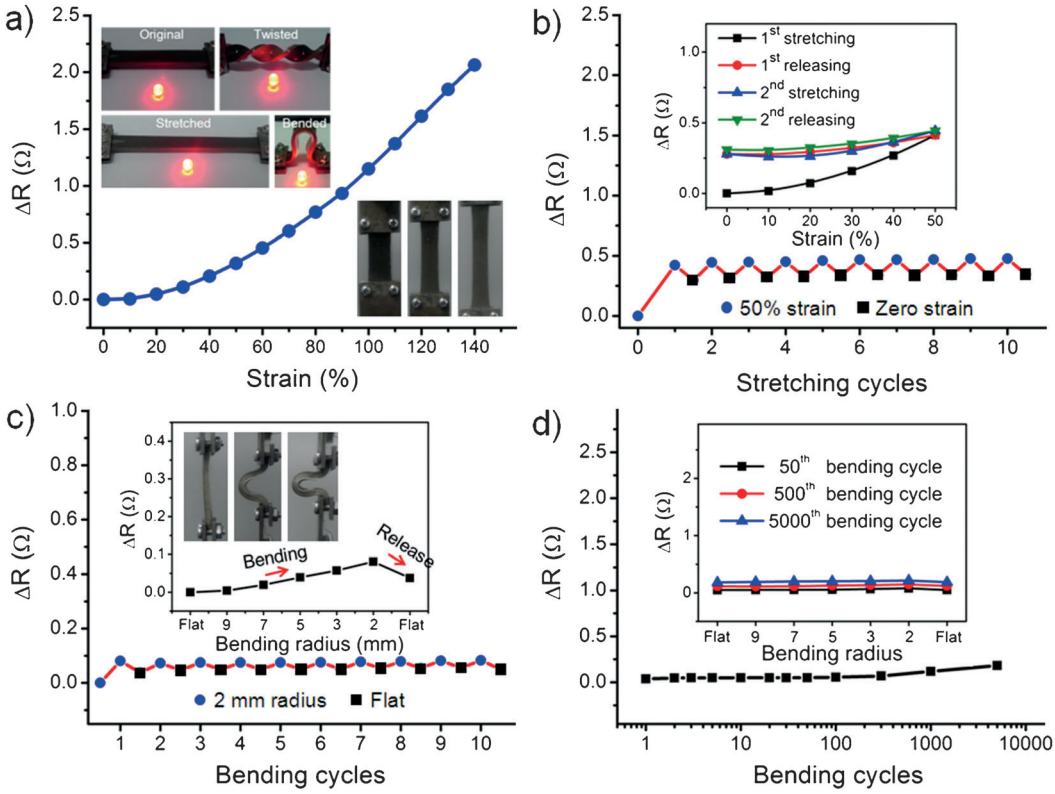

Figure 5. Electrical-resistance change of AgNWs/PDMS composites under mechanical deformation. a) ΔR of the composite as a function of uniaxial tensile strain until fracture . Left inset: photographs of the device for lightening a commercial LED using the AgNWs/PDMS composites. Right inset: photographs of the stretching process. b) ΔR of a composite after 50% stretching and then releasing for each cycle with the same stretching rate of 1 mm min^{-1}. Inset: the ΔR of the composite as a function of tensile strain up to 50% in the first two stretch-release cycles. c) ΔR of a composite when bending to a radius of 2.0 mm and then straightening for each cycle. Inset: the composite at a bend radius of up to 2.0 mm in the first bending cycle; photographs show the bending process. d) ΔR as a function of the bend cycles at a maximum bend radius of 2.0 mm. Inset: the fiftieth, five hundredth, five thousandth bending cycles. The loading of AgNWs in the PDMS matrix is about 1.5 wt% for all the measured composites and the original average resistance of all the tested samples was about 0.8 Ω. ΔR refers to the resistance change of the bent or stretched composite relative to that of the pristine composite. The size of all the measured samples is 3.7×1.2×0.2 cm^3.

nating ordered binary-network microstructure, which can be readily tuned by changing the fabrication condition. The 3D binary-network architecture has advantageous structural properties and high electrical conductivity. The tunability of the network structure together with its electrical properties should make this macroscopic 3D AgNW architecture and its composites suitable candidates in electronic applications. As a potential application, we have made this network into stretchable and foldable conductor and its electromechanical stability has been demonstrated. Furthermore, this ice-template assembly method is versatile and shows high efficiency and controllability, which may be used as a general strategy for assembly of other nanowires into advanced macroscopic 3D architectures.

Received: January 16, 2014
Revised: February 14, 2014
Published online: March 28, 2014

Keywords: conducting materials · ice · hierarchical structures · silver nanowires · template assembly

[1] a) Y. G. Sun, *Nanoscale* **2010**, *2*, 1626; b) C. Yang, H. W. Gu, W. Lin, M. M. Yuen, C. P. Wong, M. Y. Xiong, B. Gao, *Adv. Mater.* **2011**, *23*, 3052; c) Y. N. Xia, P. D. Yang, Y. G. Sun, Y. Y. Wu, B. Mayers, B. Gates, Y. D. Yin, F. Kim, Y. Q. Yan, *Adv. Mater.* **2003**, *15*, 353; d) R. S. Devan, R. A. Patil, J. H. Lin, Y. R. Ma, *Adv. Funct. Mater.* **2012**, *22*, 3326; e) Y. Z. Long, M. Yu, B. Sun, C. Z. Gu, Z. Y. Fan, *Chem. Soc. Rev.* **2012**, *41*, 4560; f) M. H. Huang, S. Mao, H. Feick, H. Q. Yan, Y. Y. Wu, H. Kind, E. Weber, R. Russo, P. D. Yang, *Science* **2001**, *292*, 1897; g) C. K. Chan, H. L. Peng, G. Liu, K. McIlwrath, X. F. Zhang, R. A. Huggins, Y. Cui, *Nat. Nanotechnol.* **2008**, *3*, 31; h) B. Z. Tian, X. L. Zheng, T. J. Kempa, Y. Fang, N. F. Yu, G. H. Yu, J. L. Huang, C. M. Lieber, *Nature* **2007**, *449*, 885; i) W. Lu, C. M. Lieber, *Nat. Mater.* **2007**, *6*, 841; j) J. F. Wang, M. S. Gudiksen, X. F. Duan, Y. Cui, C. M. Lieber, *Science* **2001**, *293*, 1455.

[2] a) J. W. Liu, H. W. Liang, S. H. Yu, *Chem. Rev.* **2012**, *112*, 4770; b) H. W. Liang, J. W. Liu, H. S. Qian, S. H. Yu, *Acc. Chem. Res.* **2013**, *46*, 1450; c) J. W. Liu, J. H. Zhu, C. L. Zhang, H. W. Liang, S. H. Yu, *J. Am. Chem. Soc.* **2010**, *132*, 8945; d) J. W. Liu, W. R. Huang, M. Gong, M. Zhang, J. L. Wang, J. Zheng, S. H. Yu, *Adv. Mater.* **2013**, *25*, 5910; e) J. W. Liu, J. Xu, H. W. Liang, K. Wang, S. H. Yu, *Angew. Chem.* **2012**, *124*, 7538; *Angew. Chem. Int. Ed.* **2012**, *51*, 7420; f) J. W. Liu, J. L. Wang, W. R. Huang, L. Yu, X. F. Ren, W. C. Wen, S. H. Yu, *Sci. Rep.* **2012**, *2*, 987; g) H. L. Gao, Y.

Lu, L. B. Mao, D. An, L. Xu, J. T. Gu, F. Long, S. H. Yu, *Mater. Horiz.* **2014**, *1*, 69; h) R. K. Joshi, J. J. Schneider, *Chem. Soc. Rev.* **2012**, *41*, 5285; i) Z. L. Wang, J. H. Song, *Science* **2006**, *312*, 242.

[3] a) B. Z. Tian, J. Liu, T. Dvir, L. H. Jin, J. H. Tsui, Q. Qing, Z. G. Suo, R. Langer, D. S. Kohane, C. M. Lieber, *Nat. Mater.* **2012**, *11*, 986; b) C. Pang, G. Y. Lee, T. I. Kim, S. M. Kim, H. N. Kim, S. H. Ahn, K. Y. Suh, *Nat. Mater.* **2012**, *11*, 795; c) K. H. Kim, Y. Oh, M. F. Islam, *Nat. Nanotechnol.* **2012**, *7*, 562; d) R. T. Olsson, M. A. S. A. Samir, G. Salazar-Alvarez, L. Belova, V. Strom, L. A. Berglund, O. Ikkala, J. Nogues, U. W. Gedde, *Nat. Nanotechnol.* **2010**, *5*, 584; e) H. W. Liang, Q. F. Guan, L. F. Chen, Z. Zhu, W. J. Zhang, S. H. Yu, *Angew. Chem.* **2012**, *124*, 5191; *Angew. Chem. Int. Ed.* **2012**, *51*, 5101; f) S. Nardecchia, D. Carriazo, M. L. Ferrer, M. C. Gutierrez, F. del Monte, *Chem. Soc. Rev.* **2013**, *42*, 794; g) M. Rauber, I. Alber, S. Muller, R. Neumann, O. Picht, C. Roth, A. Schokel, M. E. Toimil-Molares, W. Ensinger, *Nano Lett.* **2011**, *11*, 2304; h) J. M. Lee, J. W. Choung, J. Yi, D. H. Lee, M. Samal, D. K. Yi, C. H. Lee, G. C. Yi, U. Paik, J. A. Rogers, W. I. Park, *Nano Lett.* **2010**, *10*, 2783; i) S. Xu, Y. Qin, C. Xu, Y. G. Wei, R. S. Yang, Z. L. Wang, *Nat. Nanotechnol.* **2010**, *5*, 366; j) A. I. Hochbaum, P. D. Yang, *Chem. Rev.* **2010**, *110*, 527; k) B. Weintraub, Y. G. Wei, Z. L. Wang, *Angew. Chem.* **2009**, *121*, 9143; *Angew. Chem. Int. Ed.* **2009**, *48*, 8981.

[4] a) G. H. Yu, A. Y. Cao, C. M. Lieber, *Nat. Nanotechnol.* **2007**, *2*, 372; b) J. K. Yuan, X. G. Liu, O. Akbulut, J. Q. Hu, S. L. Suib, J. Kong, F. Stellacci, *Nat. Nanotechnol.* **2008**, *3*, 332.

[5] a) J. Zhu, H. L. Peng, C. K. Chan, K. Jarausch, X. F. Zhang, Y. Cui, *Nano Lett.* **2007**, *7*, 1095; b) J. Shi, Y. Hara, C. L. Sun, M. A. Anderson, X. D. Wang, *Nano Lett.* **2011**, *11*, 3413.

[6] J. Ge, H. B. Yao, X. Wang, Y. D. Ye, J. L. Wang, Z. Y. Wu, J. W. Liu, F. J. Fan, H. L. Gao, C. L. Zhang, S. H. Yu, *Angew. Chem.* **2013**, *125*, 1698; *Angew. Chem. Int. Ed.* **2013**, *52*, 1654.

[7] a) Z. P. Chen, W. C. Ren, L. B. Gao, B. L. Liu, S. F. Pei, H. M. Cheng, *Nat. Mater.* **2011**, *10*, 424; b) J. A. Rogers, T. Someya, Y. G. Huang, *Science* **2010**, *327*, 1603; c) Y. G. Sun, W. M. Choi, H. Q. Jiang, Y. G. Y. Huang, J. A. Rogers, *Nat. Nanotechnol.* **2006**, *1*, 201.

[8] a) S. Deville, E. Saiz, R. K. Nalla, A. P. Tomsia, *Science* **2006**, *311*, 515; b) S. Deville, E. Maire, G. Bernard-Granger, A. Lasalle, A. Bogner, C. Gauthier, J. Leloup, C. Guizard, *Nat. Mater.* **2009**, *8*, 966.

[9] E. Munch, E. Saiz, A. P. Tomsia, S. Deville, *J. Am. Ceram. Soc.* **2009**, *92*, 1534.

[10] a) T. Sekitani, Y. Noguchi, K. Hata, T. Fukushima, T. Aida, T. Someya, *Science* **2008**, *321*, 1468; b) F. Xu, Y. Zhu, *Adv. Mater.* **2012**, *24*, 5117; c) P. Lee, J. Lee, H. Lee, J. Yeo, S. Hong, K. H. Nam, D. Lee, S. S. Lee, S. H. Ko, *Adv. Mater.* **2012**, *24*, 3326.

